Jurnal
Teknologi

Full Paper

THE STUDY OF OPTICAL GAIN FOR TERAHERTZ QUANTUM CASCADE LASER USING DENSITY MATRIX METHOD

Mohd Asmu'i Mohd Akil[a*], Khalid Akabli[b], Amiruddin Shaari[a], Mohd Khalid Kasmin[a], Zulkafli Othaman[a]

[a]Department of Physics, Faculty of Science, Universiti Teknologi Malaysia, 81310 UTM Johor Bahru, Johor, Malaysia
[b]Docteur En Physique Theorique Et Modelisation, France

Article history
Received
12 February 2016
Received in revised form
6 June 2016
Accepted
15 August 2016

*Corresponding author
asmui@utm.my

Graphical abstract

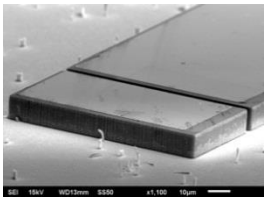

Abstract

Terahertz (THz) quantum cascade lasers (QCL) are currently increasing in popularity. It is expected to become the main source of emerging terahertz radiation technology and applications. However to produce the device within the application specification is costly and time consuming. This is because the manufacturing process of the superlattice growth and the device processing and testing are long and expensive processes. Thus a prediction tool is needed to overcome the problems in designing and producing THz QCL within the needed optical expectation. The density matrix method is used to calculate the performance of this device electronically and optically. The result obtained was compared to the experimental result conducted by previous researchers. The calculation result showed that the gain is 20 cm^{-1} when the population inversion occurs at threshold current density of 400 A cm^{-2}. Meanwhile a negative gain or loss occurs below 350 A cm^{-2}. As a conclusion, it is demonstrated that this method has a capability to explain the transport phenomena as well as to predict the performance of the THz QCL device design.

Keywords: Terahertz source, unipolar semiconductor lasers, intersubband transition, quantum cascade laser

Abstrak

Kini, Laser Terahertz Kuantum Melata sedang meningkat popular. Ia dijangka akan menjadi sumber utama dalam teknologi sinaran terahertz berserta aplikasinya. Tetapi, untuk menghasilkan peranti yang memenuhi spesifikasi pengguna adalah menelan belanja dan memakan masa. Ini adalah disebabkan proses pembuatan bagi tumbuhan kekisilampau dan peralatan pemproses serta ujian adalah proses yang panjang dan mahal. Sebab itulah peralatan ramalan diperlukan untuk mengatasi masalah berhubung penghasilan laser Terahertz Kuantum Melata dalam jangkaan optikal yang diperlukan. Kaedah ketumpatan matrik digunakan untuk membuat peralatan ramalan bagi mengira prestasi peranti secara elektronik dan optik. Keputusan dari kajian ini dibandingkan dengan keputusan eksperimen yang dijalankan oleh penyelidik sebelum ini. Daripada pengiraan, didapati nilai gandaan adalah 20 cm^{-1} apabila songsangan populasi berlaku bermula dari 400 A cm^{-2}. Sementara itu, gandaan negatif atau kehilangan berlaku dibawah 350 A cm^{-2}. Kesimpulannya, kebolehan teknik ini diuji dapat menerangkan fenomena pembawa disamping prestasi rekaan peranti laser Terahertz Kuantum Melata dapat diramalkan.

Kata kunci: Sumber terahertz, laser semikonduktor unipolar, transisi intersubband, laser kuantum melata

1.0 INTRODUCTION

The terahertz (THz) band is the part of electromagnetic spectrum located between photonics and electronics regions. It is a safe and harmless radiation because of its non-ionizing characteristic [1]. It can penetrate into any materials, but not to the water or metal. It promises many advantages over broad areas, especially in the field of security [2, 3, 4], spectroscopy [5, 6, 7] and medical imaging applications [8]. One of the successful THz radiation sources is a quantum cascade laser (QCL) [9, 10]. It is different from a conventional diode laser which operates through the recombination process between electrons and holes. THz QCL on the other hand operates by injecting electrons to the device and these electrons are cascaded through a series of conduction bands in a superlattice of the device.

THz QCL is an excellent device because of its performance to produce high optical output power with narrow emission linewidth and of its small size. The output characteristics of this device can also be designed to fulfill specific requirements of applications by engineering the conduction band to a specific design to be use in the THz QCL. Despite its advantages over other THz sources, improvement on the device design still poses a challenging task as the working principle of this device involves many-body quantum physics. Therefore, a computational work is needed when designing the device to predict the performance of the device and thus reducing the cost of manufacturing of such complicated device.

There are still some fundamental issues related to the working mechanism of THz QCL at microscopic levels that need some attention, in particular a role of the times of relaxation. They are known to affect the transport process inside the device thus, critically affect the performance of the device. Insufficient study and analysis on the electronic transport in THz QCL can lead to an unlasing device which makes the whole work and time spent in fabricating and testing the device become unprofitable. A density matrix method can be used to study the electronic transport in QCL to estimate or predict the electrical characteristics of its output as well as its optical performance based on light-current-voltage (L-I-V) profile. This should lead to a better understanding of the system as the method explicitly incorporates the effects of the electronic transitions responsible for the population inversion and the actual laser emission.

The simulation work to analyse the properties of the superlattice structure was pioneered by Kazarinov and Suris [11] utilizing numerical analysis. Then, the density matrix method was applied to study the transport properties of quantum cascade laser. In present research, the density matrix method for THz QCL is improved by incorporating the effects of scattering inside the device specifically to the effects of time of relaxation. This enhancement allows the population density of a particular level whenever it is populated or depopulated can be determined. The results discussed and presented in this article are generated from a computational work on a THz QCL design similar to the one studied experimentally by Kumar *et al*. [12]. The device simulated in this work is a four-level resonant tunneling THz QCL made of layers of AlGaAs (barriers) and GaAs (wells). The purpose of this study is to model the device using the density matrix method and to determine the required parameters to achieve population inversion to support laser emission. This study also generates the current-voltage (I-V) characteristic, population density and finally the gain curves for the device.

2.0 THEORETICAL FORMALISM

There are several widely used THz QCL designs such as the bound-to-continuum, the chirped superlattice and resonant phonon [13]. Each THz QCL design has its own mechanism of operation. In this study, we use resonant phonon THz QCL design. It is called a resonant phonon design because it utilizes the longitudinal optical (LO)-phonon resonance as the mechanism to depopulate the lower state of the laser and at the same time to inject the current to the adjacent upper level. THz QCL usually consists of more than 100 periods. The system used for the calculation described in this paper is a 4-level system as shown in Figure 1.

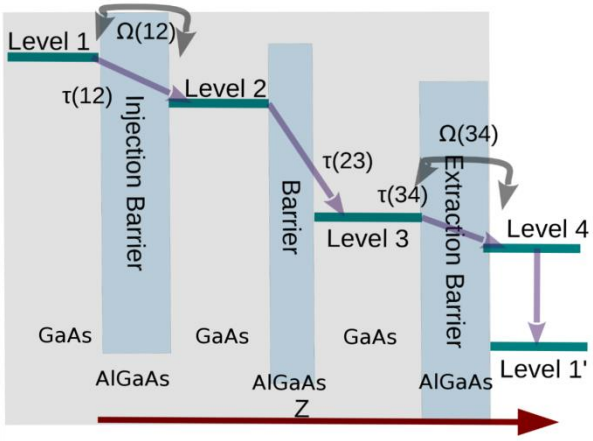

Figure 1 Illustration of conduction band diagram under bias voltage and one period of a 4-level system shaded by grey

The period consists of a GaAs layer where stated level 1 for injector, an AlGaAs layer as an injection barrier, second GaAs layer where stated level 2 upper, another AlGAs layer as a middle barrier, third GaAs layer where stated level 3 lower, and final AlGaAs layer as an extraction barrier. These periods are repeated on both sides to form several active regions for the laser. The simulation calculate the current flowing from each energy level to the neighbouring energy level. This work neglects the

effect of the stray or parasitic current, which may flow directly from level 1 to level 3. The THz radiation is produced by the transition between level 2 and level 3. The depopulation of level 4 to level 1' occurs via non-radiative transition via longitudinal optical (LO) phonon resonance. For a laser system based on GaAs, this LO-phonon has an energy of 36 meV [14].

The optical gain of a laser is defined as a relative increase of electromagnetic wave intensity per unit length as the wave propagates through the active medium [15, 16, 17]. In THz QCL, the gain comes from photons generated by laser emission in the active region within supported optical modes of the laser waveguide. Experimentally, the THz QCL gain can be measured by time domain spectroscopy [18]. Performance of THz QCL device operating at high temperature depends strongly on its gain which can be calculated and analysed only if the I-V characteristic curve of the device is known.

The analysis of the four-level system using density matrix method in this work follows the same procedures as described by other researchers [19, 20, 21, 22] applied on a three-level system with a few improvements. All the complexity of the transitions are hidden behind the terms related to the relaxation times which are often regarded as phenomenological terms. The average current density in A cm^{-2} is calculated from the expression, $j = eTr\ [\upsilon, \rho]$, where e is the charge of electon, Tr trace operator of a matrix, υ the velocity and ρ the density operator. The velocity operator in turn can be written as $\upsilon = \frac{i}{\hbar}\ [H, Z]$ where $H = H_0 + H'$, is the total Hamiltonian of the system, Z the position operator and $\hbar$ the planck constant. H_0 and H' are the unperturbed and the perturbation parts of the Hamiltonian respectively. The equation of motion or the time evolution of the density matrix ρ is written as :

$$\frac{d\rho}{dt} = -\frac{i}{\hbar}[H, \rho] \tag{1}$$

Thus, the time of evolution of the density matrix in terms of H_0 and H' can be written as:

$$\frac{d\rho}{dt} = -\frac{i}{\hbar}([H_0, \rho] + [H', \rho]) \tag{2}$$

where each commutator can be explicitly expanded as :

$$[H_0, \rho] = \left[\begin{pmatrix} E_1 & \hbar\Omega_{12} & \hbar\Omega_{13} & \hbar\Omega_{14} \\ \hbar\Omega_{12} & E_2 & \hbar\Omega_{23} & \hbar\Omega_{24} \\ \hbar\Omega_{13} & \hbar\Omega_{23} & E_3 & \hbar\Omega_{34} \\ \hbar\Omega_{14} & \hbar\Omega_{24} & \hbar\Omega_{34} & E_4 \end{pmatrix}, \begin{pmatrix} \rho_{11} & \rho_{12} & \rho_{13} & \rho_{14} \\ \rho_{21} & \rho_{22} & \rho_{23} & \rho_{24} \\ \rho_{31} & \rho_{32} & \rho_{33} & \rho_{34} \\ \rho_{41} & \rho_{42} & \rho_{43} & \rho_{44} \end{pmatrix}\right] \tag{3}$$

and

$$\frac{i}{\hbar}[H', \rho] = \tag{4}$$

$$\begin{bmatrix} \tau_1^{-1}\rho_{11} - \tau_4^{-1}\rho_{44} & \tau_{12}^{-1}\rho_{12} & \tau_{13}^{-1}\rho_{13} & \tau_{14}^{-1}\rho_{14} \\ \tau_{12}^{-1}\rho_{21} & \tau_2^{-1}\rho_{22} - \tau_3^{-1}\rho_{33} + \tau_{st}^{-1}\Delta\rho & \tau_{23}^{-1}\rho_{23} & \tau_{24}^{-1}\rho_{24} \\ \tau_{13}^{-1}\rho_{31} & \tau_{23}^{-1}\rho_{32} & -\tau_2^{-1}\rho_{22} + \tau_3^{-1}\rho_{33} - \tau_{st}^{-1}\Delta\rho & \tau_{34}^{-1}\rho_{34} \\ \tau_{14}^{-1}\rho_{41} & \tau_{24}^{-1}\rho_{42} & \tau_{34}^{-1}\rho_{43} & -\tau_1^{-1}\rho_{11} + \tau_4^{-1}\rho_{44} \end{bmatrix}$$

Thus the average current density can be determined from equation :

$$j = e\frac{i}{\hbar}Tr[[H, Z]\rho] \tag{5}$$

The density matrix above gives population densities for all of the levels. Note that E is an energy of levels, $\Delta\rho$ is the population inversion, $\rho_{22} - \rho_{33}$ and st is an abbreviation for stimulated transition. All of the Rabi oscillation frequencies Ω and time relaxation parameters, τ in perturbation H' are as described by Callebaut and Hu [23]. A current-voltage (I-V) profile can be achieved by calculating the average current density j with respect to the bias voltage, V which is set as a parameter when solving the rate equation above. Hence, the bias voltage V is part of the Hamiltonian H used in solving the envelope wavefunctions for the electrons in the active region.

To solve the optical gain, time evolution of the density operator during the laser emission is calculated by solving the following equations:

$$\frac{d\rho_{22}}{dt} = \frac{j}{e} - \rho_{22}\tau_2^{-1} - \sigma\Gamma S(\rho_{22} - \rho_{33}) \tag{6}$$

$$\frac{d\rho_{33}}{dt} = -\rho_{33}\tau_3^{-1} - \sigma\Gamma S(\rho_{33} - \rho_{22}) + \rho_{22}\tau_{23}^{-1} \tag{7}$$

$$\frac{dS}{dt} = \sigma\Gamma S(\rho_{22} - \rho_{33}) - \frac{c}{n}\alpha S \tag{8}$$

and

$$\sigma = \frac{4\pi e^2}{\epsilon_0 n} * \frac{|\mu_{23}|^2}{\lambda} * \frac{c}{n} * \frac{1}{L_p 2\gamma_{23}} \tag{9}$$

where S is the photon surface density in m^{-2}, Γ the overlap factor between the optical mode and the active region of the waveguide in percent, ϵ_0 the vacuum permittivity at $8.854 \cdot 10^{-12}$AsV^{-1}m^{-1}, γ_{23} the full width half maximum (FWHM) of the spontaneous emission line in s, α the total losses in m^{-1}, μ the element of dipole matrix in m, σ the cross section area per unit time in m^{2}s^{-1}, c the speed of light in ms^{-1}, λ the wavelength of laser in m, n is the refractive index of the medium, e the charge of electron and L_p the length of a period in m. Finally, the gain is calculated by using the following equation together with Equations 6, 7, 8, 9 above:

$$Gain = \sigma n(\rho_{22} - \rho_{33})\frac{n_{tot}}{c} \quad (10)$$

where n_{tot} is the total number of electrons per period.

3.0 METHODOLOGY

In this study, the calculation is employed by developing a simulation code using GCC (Gnu C Compiler). The computer code calculates the envelope wavefunctions from the structure or design of the laser with a defined bias voltage. The square of envelope wavefunctions gives an information of energy levels, electron probabilitiy density of levels and the interaction of all the energy levels. This information will be inputed to Equations 3 and 4 which are used to resolve the equation of motion as stated in Equation 2. The procedure to get the information of laser energy levels repeated for a certain bias voltage ranges. Finally, a current density can be calculated by using Equation 5 to produce the current-voltage profile. The code can also be used to calculate the gain profile for the THz QCL structure.

A formalism developed in this study as stated in Equations 6 to 10 is used to obtains the gain profile. For this calculation, the population density of the laser levels has been carefully studied. The important levels for the gain calculation are level 2 (upper level) and level 1 (lower level). The lasing of this structure is determined by the population inversion achieved between these levels. The parameters used in this study are the refractive index n = 3.6, overlap Γ = 0.99 and losses α is 20 cm^{-1}.

4.0 RESULTS AND DISCUSSION

The model is tested against an established resonant phonon THz QCL design studied by Kumar [12]. This design consists of sandwich thin film semiconductor layer of $Al_{0.15}Ga_{0.75}As/GaAs$. The thicknesses of the layers are 16.4/**4.8**/8.5/**2.8**/8.5/**4.2** (nm) [12] with the barriers (AlGaAs) indicate by bold fonts. The structure has four levels defined as injector level, upper level, lower level and extractor level and has 222 active region periods.

The geometry and dimension of THz QCL structure used in this calculation allow a study of the parasitic current occurring between the injector and extractor level. This study assumes possible resonant tunneling process between the injector and the upper level and between the injector and the lower level by the interface roughness. The photon emission is due to transition between the 2-3 level (upper to lower level) and the relaxation from the extractor to the next injector level using an LO-phonon resonance.

Finally, by solving the Equations (1-5), the calculated I-V is plotted as shown in Figure 2 along with the experimental I-V curve from Kumar [12]. Referring to Figure 2, the calculated I-V has almost the same pattern with the experimental result. There are few assumptions made in this calculation such as the use of a tight-binding approximation, population relaxation due to LO-phonon resonance and interface roughness scattering all at the device temperature of 0 K, whereas for the experimental result is at 9 K. This is the reason why the calculated trendline for I-V curve shows some deviation from the experimental one.

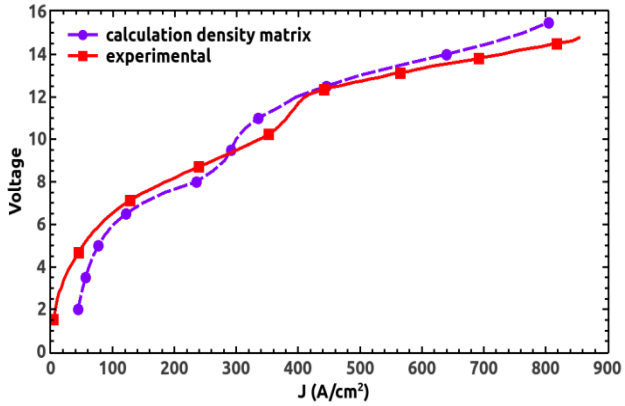

Figure 2 I-V curve extracted from the article Kumar [12] (experimental) and the result calculated using the the density matrix method

Hence, by solving Equation 2, all the levels inside the equation of motion, Figure 3 is obtained. In Figure 3, the population in injector level increases with the bias voltage change until the levels are aligned which is the condition for the electrons to tunnel through barrier. By referring to upper level density plotter in this figure, the evolution of population of level suggests that population inversion occurs at bias voltage of 11 V.

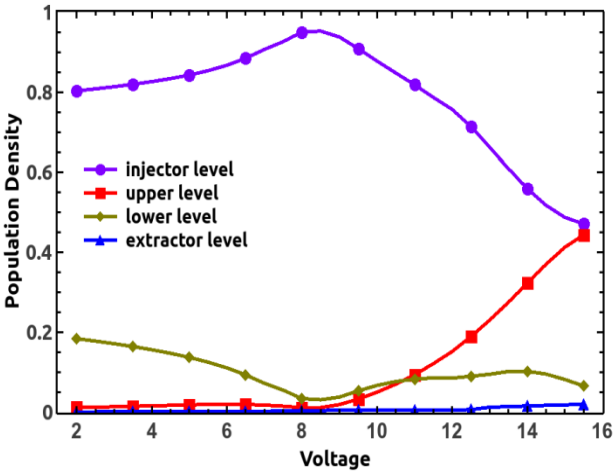

Figure 3 The evolution of population density in injector, upper, lower and extraction level by the evolution of bias, in Volt

This explains why the populations of the injector level decrease and at 9 V the populations of the upper level increase. The population inversion occurs when the upper level is highly populated than the lower level. For this inversion to occur, a good extraction mechanism is needed at the lower level to make the level always in "vacancy". If not, it will destroy the population inversion of the laser. Thus the mechanism to depopulate the lower level is by using the LO-phonon resonance, the electron transition from lower level to the adjacent active region injector level.

The THz radiation produced by the laser depends on the energy difference between level 2 and level 3. In the calculation, as the bias voltage is changed from 0 V to 16 V the level achieves population inversion, hence producing THz radiation. The frequency of the terahertz radiation produced by the device changes as the bias voltage is changed. The dependence of the optical performance of the device on the terahertz frequency usually is depicted by its gain profile. Figure 4 shows the gain evolution as the current density changes.

At the current density of about 320 A cm^{-2}, the value of gain is $0\ \mathrm{cm}^{-1}$, this is the starting point for the population inversion process. Below this current density, there is no emission produced by this THz QCL and the gain during this phase is negative. As the current density approaches the value of 350 A cm^{-2}, the threshold current density is achieved for the device to start laser emission. At this current density, the population inversion is stable enough for laser production because of the transition from level 2 (upper level) to level 3 (lower level) and then to level 4 (extractor level). The electrons in level 4 (extractor level) are being depopulated, using LO-phonon, to the next level 1' (injector level).

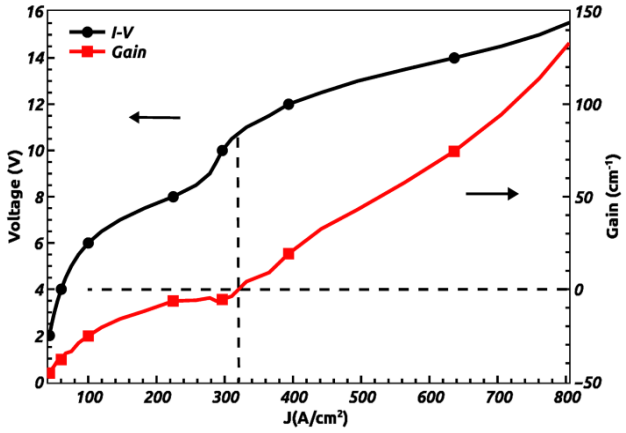

Figure 4 The calculated I-V using density matrix method and the calculated evolution of the gain for THz QCL with the change of current density

This process goes on through the entire active region. From this study, even though the population inversion starts at 320 A cm^{-2}, the transition responsible for laser emission only occurs after 350 A cm^{-2}. The current density for transition of electrons to produce laser turns out not at the same current density of the starting of the population inversion process. This is because during the starting of population inversion, the levels in this system are not aligned properly for the requirement to produce a transition to make laser emission. The level aligns properly and meets the requirement for laser transition at 400 A cm^{-2} which produces a gain value of about 20 cm^{-1}.

5.0 CONCLUSION

From this study, a prediction tool based on density matrix method which enables the computation of the current-voltage (I-V) and optical gain of THz QCL has been successfully developed. Although, the predicted I-V and gain for QCL are considered good and exhibit similar patterns compared to those from the experimental results [12], the model itself is far from perfection. This is mainly due to the approximations assumed in the calculation like the exclusion of the surface roughness and the values of times of relaxation. Further improvement can be made to this method by including the effects of coherences and other times of relaxation as well as the effect of temperature to the device.

Acknowledgement

The authors would like to acknowledge financial support from Fundamental Research Grant Scheme (vot. No. R.J130000.7826.4F244) from Ministry of Education and Universiti Teknologi Malaysia.

References

[1] Siegel, P. H. 2002. Terahertz Technology. *IEEE Transactions on Microwave Theory and Techniques.* 50(3): 910-928.

[2] Fan, W. H., Burnett, A., Upadhya, P. C., Cunningham, J., Linfield, E. H. and Davies, G. 2007. Far-infrared Spectroscopic Characterization of Explosives for Security Applications Using Broadband Terahertz Time-domain Spectroscopy. *Applied Spectroscopy.* 61(6): 638-643.

[3] Burnett, A. D., Fan, W., Upadhya, P. C., Cunningham, J. E., Hargreaves, M. D., Munshi, T., Edwards, H. G. M., Linfield, E. H. and Davies, G. 2009. Broadband Terahertz Time-domain Spectroscopy of Drugs-of-Abuse and the Use of Principal Component Analysis. *Analyst*. 134: 1658-1668.

[4] Leahy-Hoppa, M. R., Fitch, M. J. and Osiander, R. 2009. Terahertz Spectroscopy Techniques for Explosives Detection. *Analytical and Bioanalytical Chemisty.* 395(2): 247-257.

[5] Jepsen, P. U., Cooke, D. G. and Koch, M. 2011. Terahertz Spectroscopy and Imaging – Modern Techniques and Applications. *Laser & Photonics Reviews.* 5(1): 124-166.

[6] Hübers, H. W., Eichholz, R., Pavlov, S. G. and Richter, H. 2013. High Resolution Terahertz Spectroscopy with Quantum Cascade Lasers. *Journal of Infrared, Millimeter, and Terahertz Waves*. 34(5-6): 325-341.

[7] Wang, Y., Soskind, M. G., Wang, W. and Wysocki, G. 2014. High-Resolution Multi-Heterodyne Spectroscopy Based on

Fabry-Perot Quantum Cascade Lasers. *Applied Physics Letters.* 104(3): 031114-5.
[8] Tonouchi, M. 2007. Cutting-edge Terahertz Technology. *Nature Photonics.* 1: 97-105.
[9] Faist, J., Capasso, F., Sivco, D. and Sirtori, C. 1994. Quantum Cascade Laser. *Science*. 264: 553-556.
[10] Kohler, R., Tredicucci, A., Beltram, F., Beere, H., Linfield, E., Davies, G., Ritchie, D., Iotti, R. and Rossi, F. 2003. Terahertz Semiconductor Heterostructure Laser. *Physics of Semiconductors 2002, Proceedings.* 171: 145-152.
[11] Kazarinov, R. F. and Suris, R. A. 1971. Possibility of the Amplification of Electromagnetic Waves In a Semiconductor With a Superlattice. *Soviet Physics - Semiconductors.* 5: 707-709.
[12] Kumar, S., Hu, Q. and Reno, J. L. 2009. 186 K Operation of Terahertz Quantum-Cascade Lasers Based on a Diagonal Design. *Applied Physics Letters.* 94(13): 131105-3.
[13] Williams, B. S. 2007. Terahertz Quantum-Cascade Lasers. *Nature Photonics*. 1: 517-525.
[14] Strauch, D. and Dorner, B. 1999. Phonon Dispersion In GaAs. *Journal of Physics: Condensed Matter*. 2(6): 1457-1474.
[15] Banit, F., Lee, S. C., Knorr, A. and Wacker, A. 2005. Self-Consistent Theory of the Gain Linewidth for Quantum-Cascade Lasers. *Applied Physics Letters.* 86(4): 041108-3.
[16] Martl, M., Darmo, J., Deutsch, C., Brandstetter, M., Andrews, A. M., Klang, P., Strasser, G. and Unterrainer, K. 2011. Gain and Losses In THz Quantum Cascade Laser With Metal-Metal Waveguide. *Optics Express*. 19(2): 733-738.
[17] Nelander, R. and Wacker, A. 2008. Temperature Dependence of the Gain Profile for Terahertz Quantum Cascade Lasers. *Applied Physics Letters.* 92(8): 081102-3.
[18] Jukam, N., Dhillon, S. S., Oustinov, D., Zhao, Z. Y., Hameau, S., Tignon, J., Barbieri, S., Vasanelli, A., Filloux, P., Sirtori, C. and Marcadet, X. 2008. Investigation of Spectral Gain Narrowing In Quantum Cascade Lasers Using Terahertz Time Domain Spectroscopy. *Applied Physics Letters.* 93(10): 101115-3.
[19] Kumar, S. and Hu, Q. 2009. Coherence of Resonant-Tunneling Transport In Terahertz Quantum-Cascade Lasers. *Physical Review B - Condensed Matter and Materials Physics.* 80(24): 245316-14.
[20] Köhler, R., Iotti, R. C., Tredicucci, A. and Rossi, F. 2001. Design and Simulation of Terahertz Quantum Cascade Lasers. *Applied Physics Letters.* 79(24): 3920-3.
[21] Terazzi, R. and Faist, J. 2010. A Density Matrix Model of Transport and Radiation In Quantum Cascade Lasers. *New Journal of Physics.*12(3): 033045-10.
[22] Dupont, E., Fathololoumi, S. and Liu, H. C. 2010. Simplified Density-Matrix Model Applied To Three-Well Terahertz Quantum Cascade Lasers. *Physical Review B - Condensed Matter and Materials Physics.* 81(20): 205311-18.
[23] Callebaut, H. and Hu, Q. 2005. Importance Of Coherence for Electron Transport In Terahertz Quantum Cascade Lasers. *Journal of Applied Physics.* 98(10): 104505-11.